Bulletin of Electrical Engineering and Informatics
Vol. 15, No. 4, August 2026, pp. 2920~2934
ISSN: 2302-9285, DOI: 10.11591/eei.v15i4.12131

Fault detection and diagnosis in three phase IM using DSP: hardware implementation and real-time approach

Mohan P. Thakre[1], Badal Kumar[2], Supriya Nilesh Thakur[3], Alok Kumar[4], Padmini Sharma[5], Prashant Kedarnath Magadum[6]
[1]Department of Electrical Engineering, Walchand College of Engineering, Sangli, India
[2]Department of Electrical Engineering, School of Electrical and Communication Sciences, JSPM University, Pune, India
[3]Department of Electrical Engineering, Marathawada Mitra Mandal's College of Engineering, Pune, India
[4]Department of Electrical and Electronics Engineering, Government Engineering College, Raipur, India
[5]Department of Electrical and Electronics Engineering, Chhatrapati Shivaji Institute of Technology, Durg, India
[6]Department of Electrical Engineering, Brahmdevdada Mane Institute of Technology, Solapur, India

Article Info

Article history:

Received Dec 13, 2025
Revised May 16, 2026
Accepted Jun 19, 2026

Keywords:

Broken bar rotor
Digital signal processing
End ring fault
Fault diagnosis
Inter-turn fault
Real-time monitoring

ABSTRACT

The study investigates real-time problem diagnosis of induction motors (IMs) with digital signal processing (DSP) to improve monitoring. IMs are essential to industrial applications but can fail owing to mechanical, electrical, and thermal stressors. These defects must be detected quickly to prevent motor failure and production downtime. DSP is used to create a sophisticated real-time online condition monitoring system to diagnose three-phase IM issues. The suggested system was validated using MATLAB calculations and experimental investigations on a 415 V, 1 HP, 50 Hz, 1440 rpm, 4-pole IM. Disruptions in the stator windings, such as inter-turn short circuits or inter-phase faults, as well as problems with the rotor, such as broken bars or end rings, are identified in this investigation. Keeping an eye on negative sequence currents and analyzing fault frequencies with a fast Fourier transform (FFT). According to the results of the testing, current approaches are not very good at detecting stator inter-turn difficulties under light-load and no-load conditions. Under varying loads, the proposed DSP-based system identified stator inter-turn, inter-phase, and broken rotor bar problems. Results showed that the DSP-based online condition monitoring system was more accurate and better at detecting faults than earlier methods, making it a good fit for usage in industrial applications.

Corresponding Author:

Mohan P. Thakre
Department of Electrical Engineering, Walchand College of Engineering
Sangli-416415, Maharashtra, India
Email: mohanthakre@gmail.com

1. INTRODUCTION

Impellers that is induction motors (IMs) are fundamental components of commercial machinery and play a crucial role in power plants and manufacturing facilities. Given their reliance on these systems, reliability and performance are of utmost importance [1]. The timely identification of motor failures facilitates scheduled maintenance and prevents expensive production interruptions. Safety, reliability, efficiency, and performance are essential for the operation of IM systems [2]. Condition monitoring and problem diagnostics in industrial machinery are increasingly critical as the demand for system reliability escalates [3]. Fault diagnosis and condition monitoring systems can be categorized as offline and online types [4]-[6]. While offline methods require disconnecting the motor from the power source for assessment, they present considerable constraints. Examples include production disruptions, income loss, maintenance costs, and delays in service restoration [7]. Considerable interest and investigation have been directed toward online fault detection technologies capable of identifying faults without the need for motor shutdown [8], [9]. These devices enhance the efficiency of motor health monitoring compared to traditional offline methods. Investigations into fault detection and monitoring have concentrated on the squirrel-cage IM, which is a prevalent device in industrial applications [10], [11]. Many methods for monitoring the condition of three-phase IMs necessitate the use of expensive sensors [11]-[13]. Numerous sensor systems have experienced a decline in accuracy, even with the implementation of advanced technologies [14]. Electromechanical monitoring techniques are preferred because of their affordability, accessibility, and ability to identify slight variations in motor activity [15], [16].

Conventional condition monitoring systems face challenges in identifying failure frequencies because of the similarity of fault symptoms [17]-[19]. The digital signal processing (DSP) approach is one of the most precise techniques for monitoring conditions and identifying faults [20]. Online monitoring systems leverage the capabilities of DSP techniques for immediate analysis and precise identification of faults [21], [22]. A thorough examination of the existing literature revealed numerous techniques for defect detection and diagnostics in three-phase IMs, encompassing artificial intelligence (AI)-driven approaches, such as artificial neural networks, fuzzy logic systems, and genetic algorithms [23]-[26]. Currently, signature analysis, wavelet transformations, and methods based on vibration are among the alternatives [27]. Although advancements have been made in these technologies, each approach presents unique challenges, particularly in intricate fault environments [28]-[30].

This study presents a sophisticated online condition monitoring system utilizing signal processing techniques for three-phase IMs. The primary focus is on stator winding flaws, which are prevalent and challenging to identify. Fast Fourier transform (FFT) serves as a tool for the analysis of stator current waveforms, enabling the identification of specific problem frequencies. This methodology mitigates the limitations of existing fault detection systems and enhances the performance of Ims by facilitating ongoing, real-time monitoring of motor health under varying load conditions. This investigation contributes to minimizing motor failures, enhancing operational efficiency, and decreasing industrial downtime.

The remainder of this paper is organized as follows: section 2 presents a comprehensive analysis of IMs. Section 3 describes the hardware implementation of the experimental setup in detail. Section 4 focuses on the identification of stator turn faults. Section 5 presents the findings and discussions, detailing the investigation of stator windings with two turns shorted, stator winding with four turns shorted, inter-turn and inter-phase faults in the stator, analysis of end ring faults, and assessment of broken bar rotor conditions. In summary, section 6 concludes the paper outlined in this article.

2. ANALYSIS OF INDUCTION MOTORS

Figure 1 shows the equivalent circuit of a polyphase IM. Figures 1(a) and (b) depict the equivalent circuits of a polyphase IM during the no-load and blocked rotor tests, respectively.

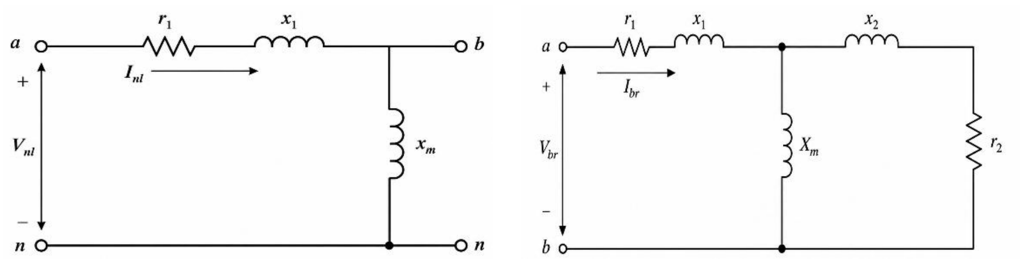

(a) (b)

Figure 1. Equivalent circuit of polyphase IM; (a) no load test and (b) at block rotor test

The stator no-load impedance is given by in (1):

$$Z_{n1} = \frac{V_{n1}}{I_{n1}^2} \quad (1)$$

The stator no-load resistance is calculated as (2):

$$R_{n1} = \frac{P_{n1}}{I_{n1}^2} \quad (2)$$

The stator no-load reactance is given in (3):

$$X_{n1} = \sqrt{z_{n1}^2 + R_{n1}^2} \quad (3)$$

where, V_n^0 is per phase voltage applied, I_n^0 is per phase input current, P_n^0 is per phase power input, s_{n1} is slip at no load=0, $X_{n1} = x_1 + X_m = X_1$, and X_1 is stator self-reactance.

In the blocked rotor test, the rotor shaft is externally blocked. Balanced polyphase voltages at the rated frequency are applied to the stator terminals through a polyphase Variac, and the applied voltage is adjusted to the rated current. The blocked rotor parameters are calculated using (4)-(12). The DC resistance per phase of the stator winding is measured shortly after this test and is calculated as given in (4)-(7):

$$r_1 = (1.1 - 1.3)r_{1dc} \quad (4)$$

The blocked rotor impedance is calculated by (5):

$$Z_{br} = \frac{v_{br}}{I_{br}} \quad (5)$$

The blocked rotor resistance is:

$$R_{br} = \frac{P_{br}}{I_{br}} \quad (6)$$

The blocked rotor reactance is:

$$X_{br} = \sqrt{z_{br}^2 - R_{br}^2} \quad (7)$$

where V_{br}, V_{br}=P_{br} are the applied voltage, I_{br} is per phase-rated current input, and P_{br} is per phase power input, respectively, per phase. From the analysis of the equivalent circuit during the blocked rotor test, the rotor reactance can be expressed as in (8)-(12):

$$X_{br} = X_1 + \frac{X_2}{1+\frac{X_2}{X_m}} \quad (8)$$

Since, $X_2 \ll x_m$, we neglect the small term $\frac{X_2}{X_m}$, resulting in $X_{br} = x_1 + x_2$.
Assume $x_1 = x_2$, we can write:

$$x_1 = x_2 = \frac{X_{br}}{2} \quad (9)$$

Also blocked rotor resistance is:

$$R_{br} = r_1 + r_2 \frac{X_m^2}{r_2^2+x_2^2} \quad (10)$$

But $X_2 \ll x_m$ this simplifies to:

$$R_{br} = r_1 + r_2 (\frac{X_m^2}{X_2}) \quad (11)$$

The per-phase rotor resistance is:

$$r_2 = (R_{br} - r_1)(\frac{X_2}{X_m})^2 \quad (12)$$

The parameters obtained from the no-load and blocked rotor tests shown in Figure 1 were used in the Simulink model of study system.

3. HARDWARE IMPLEMENTATION

The experimental setup and its results for stator and rotor defects under different conditions are detailed as shown in Figure 2. The following is a breakdown of the parameters for the three-stage IM: with a total of 160 turns per phase, this 415 V, 1 HP, 50 Hz, 1440 rpm, 4-pole, 2.1 A motor features 80 turns per coil, and two coils per phase. Experiments on winding failures were conducted using this motor, which had stator winding turns that were suitably constructed. Stator winding anomalies, including two and four inter-turn short-circuit faults, a broken one-bar rotor fault, a broken two-bar rotor fault, and broken end-ring faults, were the primary focus of the investigation. The experiments were performed under no-load, half-load, and full-load conditions. Fault frequencies were analyzed to assess the condition of the IMs.

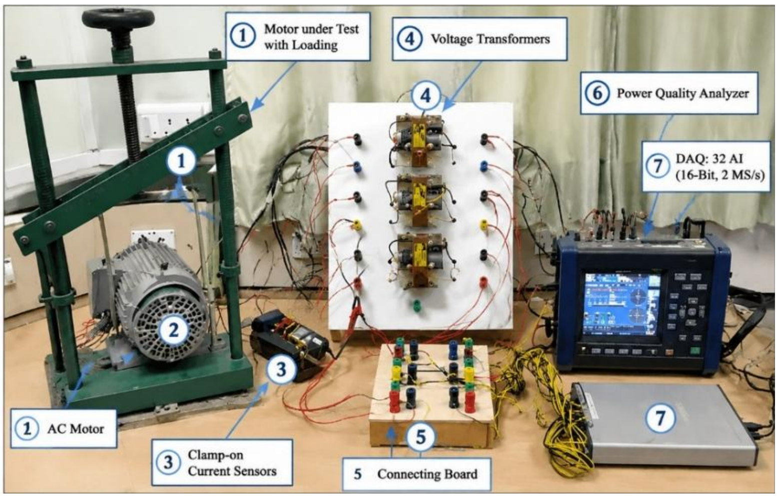

Figure 2. Experimental setup of study system

Figure 2 shows the three-phase IM stator and rotor winding fault detection experimental setup. The 415 V motor being assessed produces 1 HP at 50 Hz and 1440 rpm with four poles. Motor specifications: 80 turns per coil and two coils per phase for 160 turns per phase at 2.1 A. Specific stator winding turns were chosen for fault detection studies to test winding faults. Voltage transformers, power quality analyzers, and DAQ devices are essential. Single-phase 600 V, 50 Hz voltage transformers with a transformation ratio of 415/5 V and a burden of 0.5 VA were used. They were classified as Class-1.0/0.5. Motor electrical parameters were monitored and assessed using a Hioki 3198 power quality tester. The measurement setup included Hioki 9694 clamp-on current sensors with a 5 A current, 300 V voltage, and 10 mV per ampere output. The sensors helped observe the motor current signals.

An NI USB 6363 data acquisition system was used, which included 32 analog inputs (16-bit, 2 MS/s), four analog outputs, and 48 digital inputs/outputs. Electrical motor data were quantified and analyzed using an NI-DAQ device. The system employs NI STC3 technology, which combines digital and analog timing engines for synchronization and timing to enhance measurement precision. Motor speed data were retrieved from a digital tachometer and processed using LabVIEW. The use of these tools enabled a thorough evaluation of the motor performance under varying loads, which in turn exposed problems with the stator and rotor windings.

4. DETECTION OF STATOR TURNS FAULT

In this study, a DSP was used to detect stator winding defects in a three-phase IM. Winding problems can be detected by examining the stator current fault frequency component. The proposed technology allows for real-time stator health monitoring in motors under diverse load conditions, thereby enabling early problem detection. IEEE and EPRI have reported that stator winding insulation concerns cause 28%–36% of motor failures. An abnormality in the stator increases circulating currents, thereby elevating the winding temperature. The square of the current flow generates heat energy, which can cause motor failure. Thermal overloading, cycling, and transient voltage stress all degrade the insulation; however, thermal overloading is the primary cause. Stator insulation failure can be attributed to aging, overloading, and switching oscillations.

Even the best insulation can fail if the motor exceeds its temperature limits. A 10 °C temperature increase reduces insulation durability by 50%. Therefore, the stator winding temperature must be monitored to keep the motor within its thermal limits. Contamination can reduce the insulating performance; therefore, keeping the motor clean is essential. Stator winding defects include turn-to-turn, coil-to-coil, line-to-ground, line-to-line, and open circuits. Turn-to-turn problems are the most difficult to identify. This study uses DSP and the FFT approach to evaluate current data for fault frequency components and discover stator short-winding defects.

Figure 3 shows the DSP technique utilized in the experimental setup for detecting faults in both the stator and rotor components. The diagram depicts the methodology for acquiring current and voltage signals using clamp-on current sensors and potential transformers. The FFT extracts the magnitude and phase of the input signals, whereas the sequence filter calculates the magnitude and phase of the sequence components. This methodology offers a reliable framework for the instantaneous detection of stator winding anomalies.

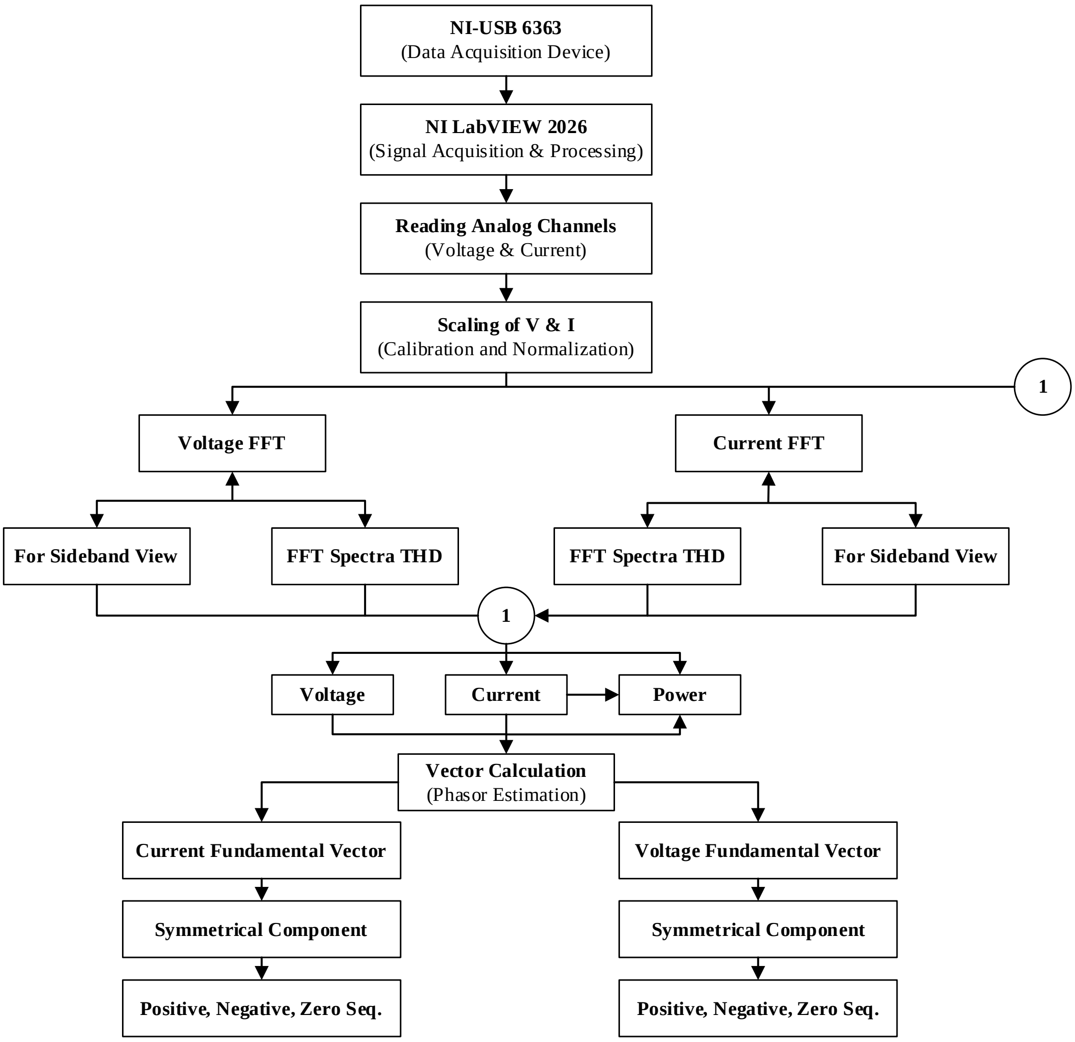

Figure 3. DSP technique

The detection of stator inter-turn faults in an IM using MCSA is based on detecting the frequency components from (13):

$$f_{st} = f_s[\frac{1-s}{p}] \quad (13)$$

where f_{st} is stator inter-turn fault frequency in Hz, fs is supply frequency in Hz, s is slip in p. u., and p is poles. First, the healthy motor was tested, and then the faulty motor was tested by introducing different types of faults. The results are presented below. The equation for fault frequency components owing to the stator short circuit is given by (14):

$$f_{st} = f_s[k + \frac{n}{p}(1-s)] \quad (14)$$

where f_{st} the frequency component owing to the inter-turn fault in the stator current, p a pair of poles (p=2), k is 1, 3=1,3,5..., n is 1, 2=1,2,3...

5. RESULTS AND DISCUSSION

To replicate stator inter-turn, short-circuit faults, phase B winding was accessed at various turns, and an external short circuit was applied across two turns of phase B. The frequency spectra of the stator current were subsequently observed using a DSP in no-load, half-load, and full-load scenarios, followed by a verification process.

5.1. Stator winding with shorted two turns

Figure 4 shows the two inter turn short at no load and half load condition. Figure 4(a) presents inter-turn shorts occurring in a no-load scenario. The motor speed was 1496 rpm under no-load conditions, with the lower-sideband and upper-sideband frequencies recorded at 25.084 Hz and 74.99 Hz, respectively. However, the spectra did not clearly show the fault frequencies. Detecting stator inter-turn short-circuit defects under no-load circumstances is challenging because of the limited current flow. Figure 4(b) shows two examples of half-load inter-turn short circuits.

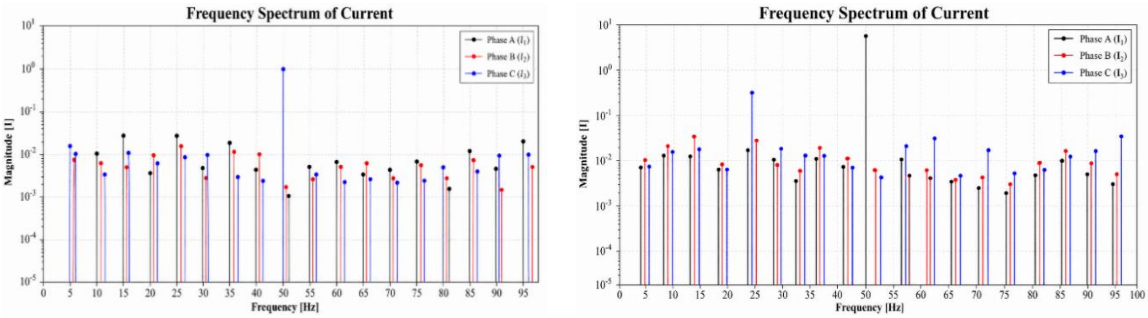

(a) (b)

Figure 4. Two inter turn short at; (a) no load and (b) half load condition

The motor displayed an operational speed of 1426 rpm and a slip value of 0.0493 under half-load conditions. The fault frequencies at lower sideband (LSB) 26.25 Hz and upper sideband (USB) 73.82 Hz could not be detected, according to the research. The expected failure frequencies under different load scenarios, together with the associated characteristics, are listed in Table 1. It is difficult to identify stator inter-turn short-circuit faults under various load situations because the fault frequencies were undetectable under the experimental configurations.

Table 1. Expected fault frequencies with two inter-turn short circuit fault

Load conditions	Speed (rpm)	Slip	k=1			
			LSB (Hz)	Observation	USB (Hz)	Observation
No load	1496	0.0026	25.084	Not visible	74.99	Visible
Half load	1426	0.0493	26.25	Not visible	73.82	Not visible

5.2. Stator winding with shorted four turns

Figure 5 represents four inter turns short at considering no load, half load and full load condition. Figure 5(a) illustrates four instances of inter-turn shorts that arise in the absence of a load. The unloaded speed was measured at 1496 rpm, whereas the frequencies for the LSB and USB were documented at 25.084 Hz and 74.99 Hz, respectively. The fault frequencies were undetectable in the frequency spectra of the stator current. Identifying stator inter-turn short-circuit faults under no-load conditions presents significant challenges. Figure 5(b) illustrates four instances of inter-turn short circuits occurring under half-load conditions. The velocity under half-load conditions was recorded at 1426 rpm, with the lower-sideband and upper-sideband frequencies determined to be 26.025 Hz and 73.82 Hz, respectively. The fault frequencies were absent in the frequency spectra of the stator current. Identifying stator inter-turn short-circuit faults under no-load conditions presents significant challenges. Figure 5(c) illustrates four occurrences of inter-turn shorts under full-load conditions.

The expected fault frequencies with four inter-turn short circuit fault is shows in Table 2. The operational speed under full-load conditions was measured at 1380 rpm, accompanied by a slip value of 0.083. The frequencies for the LSB and USB were 27.09 Hz and 77.13 Hz, respectively. The analysis of the stator current frequency spectra revealed the detectability of the LSB fault frequencies, whereas the USB fault frequencies remained undetectable. Detecting stator inter-turn short-circuit faults under full-load conditions presents significant challenges.

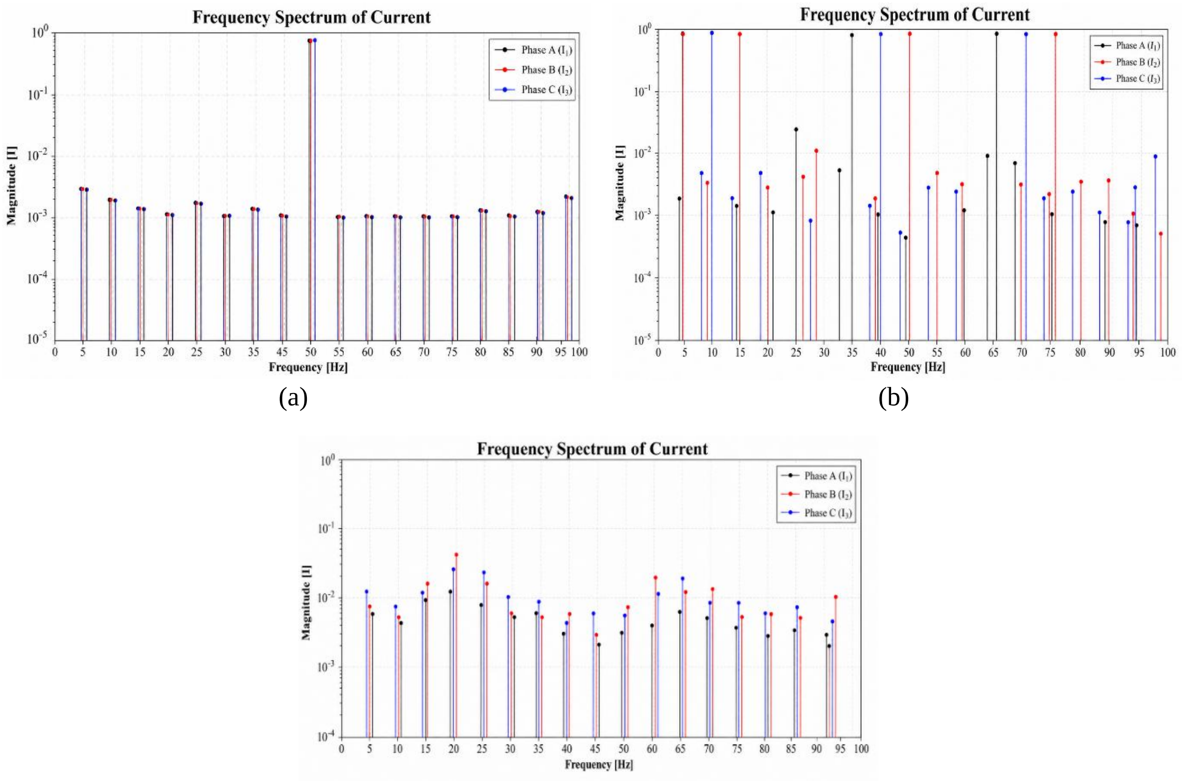

(a) (b) (c)

Figure 5. Four inter turns short at; (a) no load, (b) half load, and (c) full load condition

Table 2. Expected fault frequencies with four inter-turn short circuit fault

Load conditions	Speed (rpm)	Slip	k=1			
			LSB (Hz)	Observation	USB (Hz)	Observation
No load	1496	0.0026	25.084	Not visible	74.99	Not visible
Half load	1426	0.0493	26.25	Not visible	73.82	Not visible
Full load	1380	0.083	27.09	Visible	77.13	Not visible

5.3. Stator inter-turn inter-phase fault

Simultaneously, a short circuit was applied to two interturn windings of phases B and C. The resulting frequency spectra of the stator current under no-load, half-load, and full-load conditions are shown in Figures 6(a) to (c), respectively. Table 3 lists the exact frequency spectra of the stator current that were studied using the FFT. This method is effective for identifying stator inter-turn and inter-phase problems.

The anticipated fault frequency for a stator inter-turn inter-phase fault under various load scenarios is displayed in Table 3. Both LSB and USB fault frequencies are shown under no load, half load, and full load. Both the LSB and USB frequencies are visible at no load and half load, however only the USB is visible at full load.

5.4. Stator inter turn fault detection by negative sequence current method

A method for identifying short-circuit problems between turns in the stator is inter-turn fault detection. The negative-sequence current was computed using the FFT of the frequency spectra obtained from the stator current. The magnitudes of the currents in the negative series are listed in Table 4.

The negative-sequence current remained unchanged after shorting the two-phase turns. The FFT analysis conducted on four inter-turn short circuits within the stator current revealed a negligible fluctuation in the negative-sequence current. Various approaches have been suggested, such as negative sequence impedance, vibration analysis, noise assessment, and monitoring, to improve the identification of stator inter-turn faults.

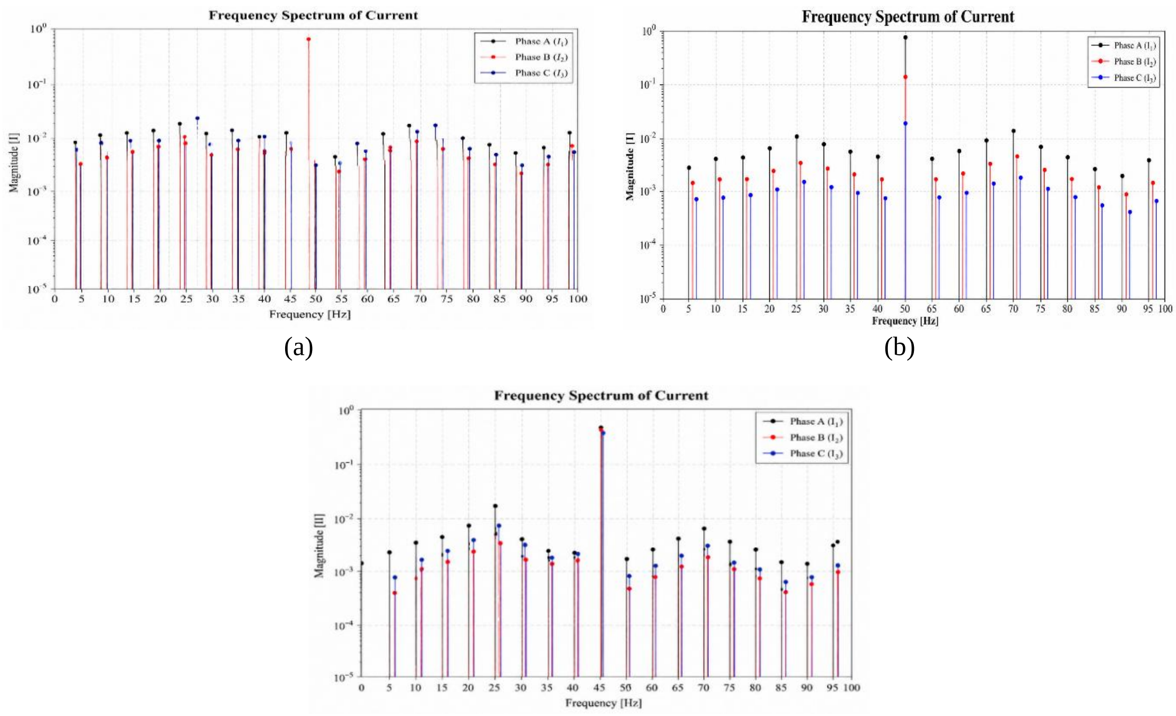

(a) (b)

(c)

Figure 6. Two inter turns short at phase B & C on; (a) no load, (b) half load, and (c) full load condition

Table 3. Expected fault frequency for stator inter-turn inter-phase fault

Load conditions	Speed (rpm)	Slip	k=1			
			LSB (Hz)	Observation	USB (Hz)	Observation
No load	1496	0.0026	25.084	Visible	74.99	Visible
Half load	1426	0.0493	26.25	Visible	73.82	Visible
Full load	1380	0.083	27.09	Not visible	77.13	Visible

Table 4. Negative sequence current at various load conditions

Load conditions	Two turns short circuited	Four turns short circuited
No load condition	0.0665	0.0794
Half load condition	0.0677	0.0847
Full load condition	-	0.0708

5.5. Broken bar rotor analysis

Along with stator fault identification, rotor fault identification is explained. Although broken rotor bars rarely cause motor failure, if ignored, they can cause significant mechanical damage, including insulation and winding damage. Repair costs and operating interruptions can be reduced via early rotor bar defect detection. Inadequacies in the rotor manufacturing process require a uniform air gap for accurate bar positioning; any imperfections may cause damage; DOL starting or frequent switching increases rotor current, which raises rotor temperatures and damages bars and end rings; and pulsating mechanical loads. Stator and bearing faults have been extensively studied; however, rotor faults have not.

Several methods for diagnosing rotor defects have emerged in the previous decade. DSP and computerized data collection can be used to detect rotor defects. FFT, STFT, and WT are used to detect rotor bar problems. Spectrum analysis is used to identify fault-related harmonics. Rotor bars with defects emit sideband frequencies near the fundamental frequency. A decibel (dB) versus frequency spectrum identifies current signature patterns that may indicate defects. In a three-phase IM, the stator generates a rotating magnetic field that causes slip frequency rotor currents. In rotor asymmetry cases, a backward-rotating field at the slip frequency generates voltage in the stator at the related frequency, which alters the stator current frequency. A balanced three-phase supply generates a synchronized forward-rotating magnetic field from the motor, as given in (15) and (16):

$$N_s = \frac{120fs}{p} \tag{15}$$

Slip:

$$s = \frac{Ns - N_r}{N_r} \tag{16}$$

where, slip speed=$Ns - Nr$, rotor speed and $Nr = Ns(1 - s)$. The backward-rotating magnetic field speed produced by the rotor owing to broken bars and with respect to the rotor is $Nr - sNs$ and, as given by (17):

$$Nsb = Ns(1 - 2s) \tag{17}$$

Above equation in terms of frequency, $fbrb = fs(1 - 2s)$.
Therefore, twice slip frequency sidebands occur at $\pm 2sf_s$ both sides of the supply frequency, as given by (18):

$$fbrb = fs(1 \pm 2s) \tag{18}$$

The LSB and USB frequencies produce oscillations in speed and torque, resulting in increased mechanical stress on the bearings. The sequence of the sideband frequency can be observed in (19):

$$fbrb = fs(1 \pm 2ks) \tag{19}$$

where, k=1,2,3.

5.5.1. One broken bar fault

Figure 7 shows the current frequency spectra from the current signal for a single broken bar at no load, half load, and full load. As shown in Figure 7(a), the sideband frequency is close to the fundamental frequency and has low sideband amplitudes in the absence of load. Owing to the low current in the rotor bars, detecting the slip frequency sideband under no load is difficult. Figure 7(b) indicates that the sideband fault frequencies are sufficiently low to be difficult to detect, even under half load. Thus, detecting broken rotor bar problems under half-load circumstances is difficult. The motor speed under load significantly affects the sideband frequency. At half load, the sideband frequencies become visible because the experimental motor has a low rating, thereby reducing the speed under load. As shown in Figure 7(c), the fault frequencies of a single broken bar are only visible when the motor is at 80% or full load. Table 5 lists the frequencies of broken-bar rotor defects.

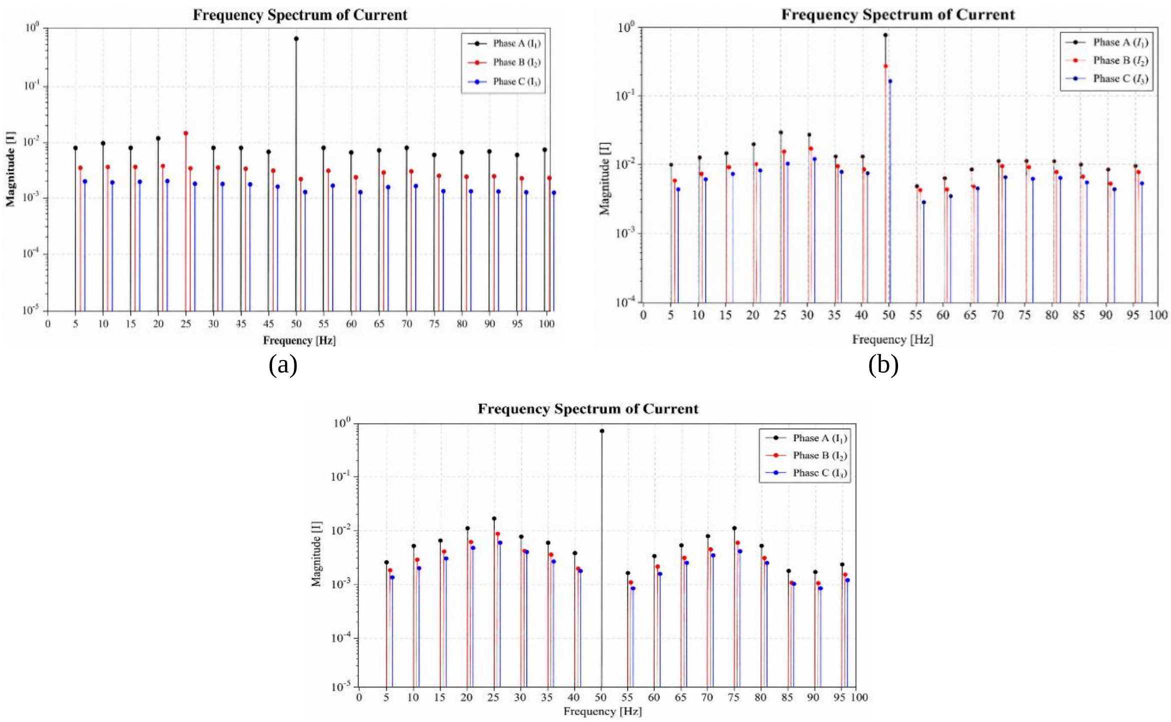

Figure 7. Frequency spectra for stator current for one bar broken at; (a) no load, (b) half load, and (c) full load condition

Table 5. Expected fault frequencies with one broken bar under various conditions

Load conditions	Slip	Fault frequencies							
		k=1				k=2			
		LSB (Hz)	Observation	USB (Hz)	Observation	LSB (Hz)	Observation	USB (Hz)	Observation
No load	0.0026	49.77	Not visible	50.298	Not visible	49.51	Not visible	50.55	Not visible
Half load	0.0493	45.104	Visible	54.97	Visible	40.17	Visible	59.9	Visible
Full load	0.083	41.731	Not visible	58.344	Visible	33.42	Visible	66.65	Visible

Figure 7 shows the no-load frequency spectrum of the current of a healthy motor. A cracked rotor bar under no-load is shown in Figure 7(a). Under no load, the speed was 1496 rpm, and the LSB and USB frequencies were 49.77 Hz and 50.298 Hz, respectively. The absence of these fault frequencies in the stator current frequency spectra makes it difficult to detect a broken rotor bar fault under no-load conditions. Figure 7(b) shows a half-loaded cracked rotor bar. At half load, the rotational speed was 1426 rpm, and the LSB and USB frequencies were 45.104 and 54.97 Hz, respectively. The stator current frequency spectra revealed the fault frequencies, facilitating the identification of a fractured rotor bar defect. Figure 7(c) shows a cracked rotor bar under the maximum load. The full-load speed was 1380 rpm, and the LSB and USB frequencies were 41.731 and 58.344 Hz, respectively. The LSB was not present in the stator current frequency spectra, whereas the USB was present, suggesting that diagnosing a broken rotor bar fault under full-load conditions is difficult.

5.5.2. Two broken bar faults

Table 6 analyses the current frequency spectra for two damaged rotor bars under no-load, half-load, and full-load conditions. Figure 8 shows the frequency spectra of the current signals of the two damaged bars under load. As shown in Figure 8(a), fault frequencies near the fundamental frequency have insignificant amplitudes and are undetectable without a load. Detecting a fault is difficult in the rotor bars because of the low current when the motor is running at no or mild load. Figure 8(b) shows the half-load current spectrum of the motor with two broken bars. The low magnitudes of the fault frequencies make it difficult to detect a broken-bar fault during the half-load. Figure 8(c) shows the full-load power spectrum of the motor with two broken bars. The frequencies of 58.344 Hz and 33.42 Hz confirm a fractured rotor bar issue.

Table 6. The expected fault frequencies with two broken bars at various load conditions

Load conditions	Slip	Fault frequencies							
		k=1				k=2			
		LSB (Hz)	Observation	USB (Hz)	Observation	LSB (Hz)	Observation	USB (Hz)	Observation
No load	0.0026	49.77	Not visible	50.298	Not visible	49.51	Not visible	50.55	Not visible
Half load	0.0493	45.104	Not visible	54.97	Not visible	40.17	Not visible	59.9	Not visible
Full load	0.083	41.731	Not visible	58.344	Visible	33.42	Visible	66.65	Not visible

5.6. End ring fault analysis

The same materials are used to fabricate the end rings that join the rotor bars. Because all rotor bar currents flow into the end ring, the rotor current is considerably higher than the stator current. Therefore, the end ring current is considerably higher than that of the rotor bars. The end rings are larger than the rotor bars to support high current flow. Figure 9(a) shows a fractured end-ring fault under no-load conditions, with LSB and USB values of 49.77 Hz and 50.298 Hz, respectively. The absence of LSB and USB components in the stator current frequency spectra hampers fault diagnosis under no-load conditions. Similarly, Figure 9(b) shows a fractured end-ring fault under half-load conditions, with LSB and USB values of 45.104 Hz and 54.97 Hz, respectively. Again, neither the LSB nor USB was observed in the stator current frequency spectra, demonstrating that locating the fault under half-load conditions is difficult.

Figure 9 shows the frequency spectrum of a damaged end-ring fault at full load, with an LSB at 41.731 Hz and a USB at 58.344 Hz. The stator current frequency spectrum has a recognizable bottom sideband but no higher sideband, making defect diagnosis difficult. Figure 9 shows the fractured end-ring fault frequency spectra under no-load, half-load, and full-load conditions. The sideband frequencies aligned closely with the fundamental frequency in the absence of a load, but their amplitudes were significantly reduced (Figure 9(a)). The minimal current of the end ring makes slip-frequency sideband identification difficult under no-load conditions. As shown in Figure 9(b), 40.17 Hz was recorded at half load, although other frequencies related to the same issue may be undetected. Thus, detecting a fractured end-ring fault during half-load remains challenging. The sideband frequency and motor speed under load are related, with fault frequency sidebands for the end ring only visible at 80% or full load, as shown in Figure 9(c). The fault frequencies under full load were 41.731 Hz and 66.65 Hz, confirming a broken end-ring problem. The difficulty of detecting broken end-ring faults, specifically differentiating them from broken rotor bar faults, is seen in Table 7.

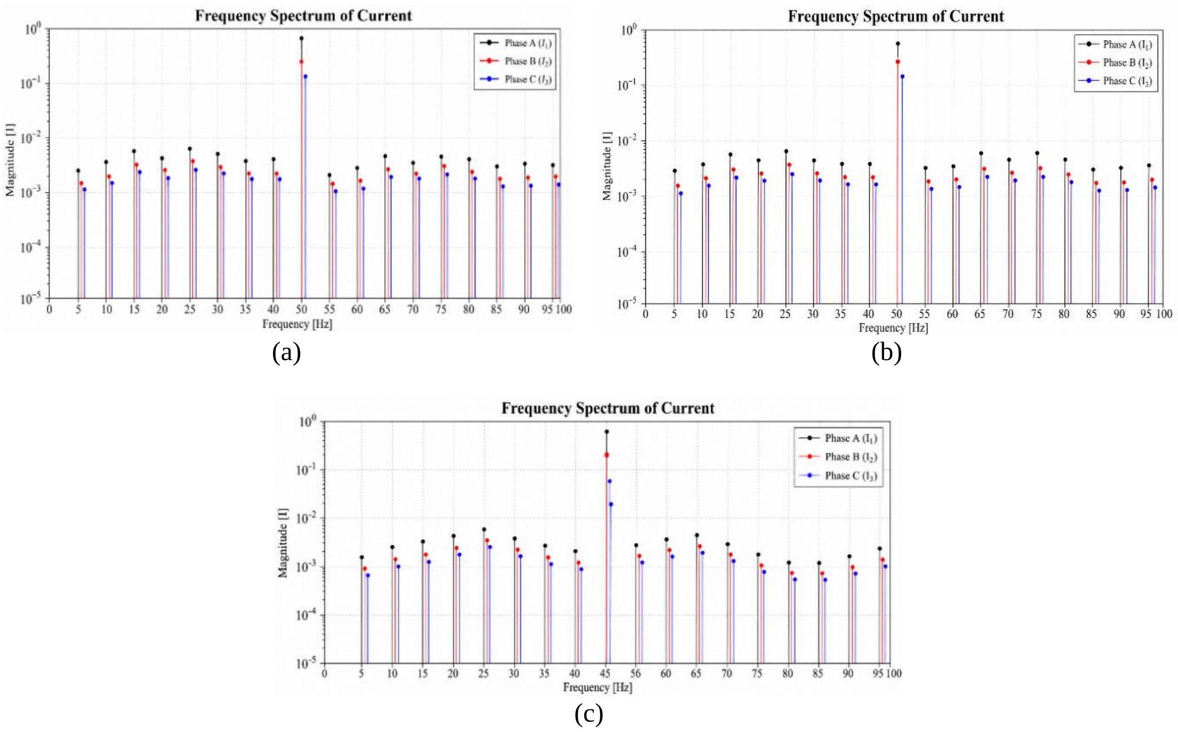

Figure 8. Frequency spectra for stator current for two bars broken at; (a) no load, (b) half load, and (c) full load condition

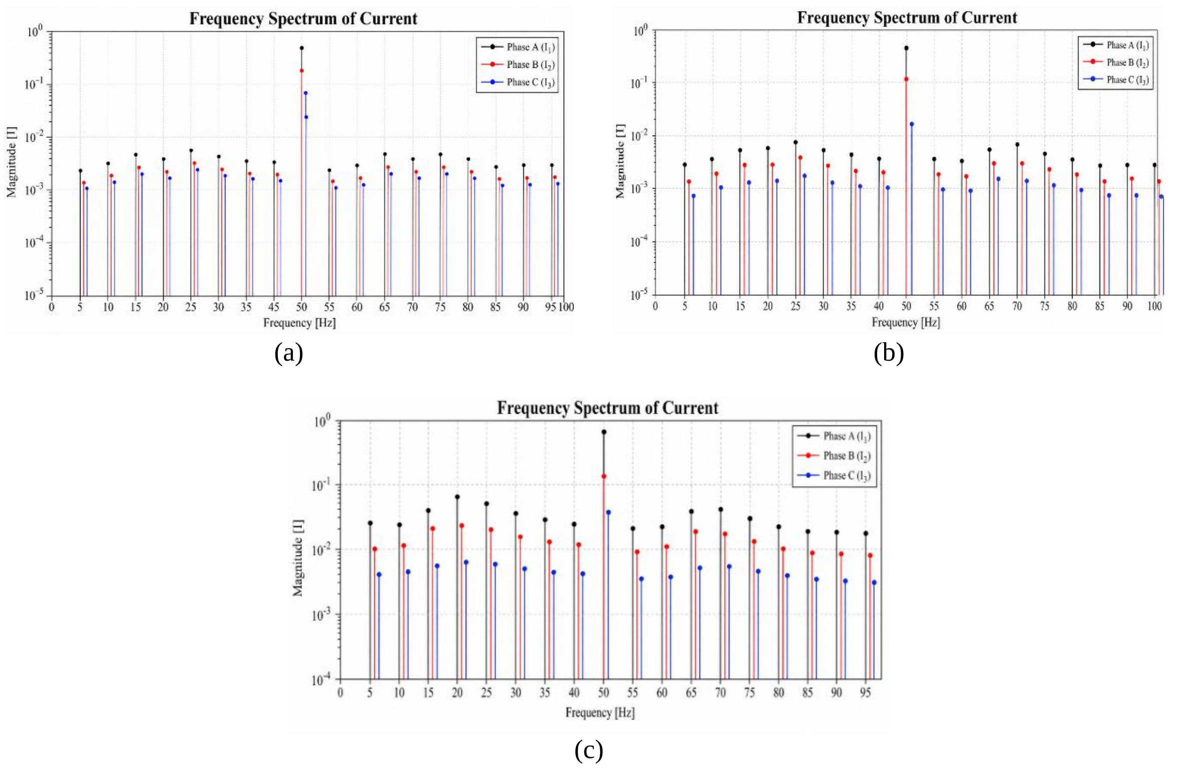

Figure 9. Frequency spectra for stator current for end ring at; (a) no load, (b) half load, and (c) full load

Table 7. The expected fault frequencies with broken end ring various load conditions

Load conditions	Slip	Fault frequencies							
		k=1				k=2			
		LSB (Hz)	Observation	USB (Hz)	Observation	LSB (Hz)	Observation	USB (Hz)	Observation
No load	0.0026	49.77	Not visible	50.298	Not visible	49.51	Not visible	55.24	Not visible
Half load	0.0493	45.104	Not visible	54.97	Not visible	40.17	Visible	59.9	Not visible
Full load	0.083	41.731	Visible	58.344	Not visible	33.42	Not visible	66.65	visible

For both LSB and USB frequencies at various slip values (k=1, k=2), the table displays fault frequencies for broken end-ring faults under a variety of load conditions, including no load, half load, and full load. All fault frequencies are invisible when there is no load. The LSB frequency for k=2 is visible at half load, but the USB frequencies for k=1 and k=2 are not. Other frequencies are not visible at full load, however the LSB for k=1 and USB for k=2.

6. CONCLUSION

This study explores the use of negative-sequence current analysis for three-phase IM fault detection. The findings demonstrate that negative-sequence currents can be utilized to identify stator short circuits and create torque oscillations that stress motor bearings. Significant negative-sequence current values of 1.887 A and 2.566 A under various fault circumstances were found in the simulation findings. Nevertheless, the findings of the experiment showed that it was difficult to identify stator inter-turn short-circuit flaws under no-load and half-load situations, but it was easier to do so under full load.

Under specific operating conditions, the investigation also revealed challenges in detecting minor defects like two-turn short circuits and rotor problems like broken rotor bars. Future research on wavelet-based fault diagnostic systems is suggested by the paper, with an emphasis on light-load fault diagnosis and the use of hybrid DSP machine learning techniques. The reliability of detection could be further increased by integration with cloud-based or remote monitoring systems. In sectors like mining and oil refining, where early motor defect identification is essential for reducing downtime and preserving operating efficiency, these developments are especially helpful for remote surveillance.

ACKNOWLEDGMENTS

The authors gratefully acknowledge the valuable guidance and technical support provided by Walchand College of Engineering, Sangli, Maharashtra, India whose insights greatly contributed to the successful completion of this work.

FUNDING INFORMATION

Authors state no funding involved.

AUTHOR CONTRIBUTIONS STATEMENT

This journal uses the Contributor Roles Taxonomy (CRediT) to recognize individual author contributions, reduce authorship disputes, and facilitate collaboration.

Name of Author	C	M	So	Va	Fo	I	R	D	O	E	Vi	Su	P	Fu
Mohan P. Thakre	✓	✓	✓	✓	✓	✓	✓		✓	✓	✓	✓		
Badal Kumar	✓			✓		✓	✓			✓		✓		
Supriya Nilesh Thakur		✓			✓	✓		✓	✓					
Alok Kumar		✓		✓		✓				✓				
Padmini Sharma		✓			✓			✓	✓		✓			
Prashant Kedarnath Magadum	✓		✓			✓				✓	✓	✓		

C : **C**onceptualization
M : **M**ethodology
So : **So**ftware
Va : **Va**lidation
Fo : **Fo**rmal analysis
I : **I**nvestigation
R : **R**esources
D : **D**ata Curation
O : Writing - **O**riginal Draft
E : Writing - Review & **E**diting
Vi : **Vi**sualization
Su : **Su**pervision
P : **P**roject administration
Fu : **Fu**nding acquisition

CONFLICT OF INTEREST STATEMENT

Authors state no conflict of interest.

INFORMED CONSENT

We have obtained informed consent from all individuals included in this study.

DATA AVAILABILITY

Data availability is not applicable to this paper as no new data were created or analyzed in this study.

REFERENCES

[1] U. P. Da Costa, A. Pelizari, E. C. M. Da Costa, and G. R. Bruzinga, "Comparative Analysis in Single-Phase Induction Motors: Analytical, Numerical, and Load Tests," *IEEE Access*, vol. 13, pp. 180578–180592, 2025, doi: 10.1109/ACCESS.2025.3622064.

[2] S. Jiang, Z. Sun, X. Zhu, Z. Hu, and Y. Du, "Real-Time Rotor Temperature Estimation of Induction Machines Using a Differentiated Input Thermal Neural Network," *IEEE Transactions on Transportation Electrification*, vol. 11, no. 6, pp. 14009–14022, 2025, doi: 10.1109/TTE.2025.3607350.

[3] Z. Jia, W. Song, C. Ma, B. Zhang, and N. Sun, "An MPC-Based Online Interturn Fault Diagnosis Method for Induction Motors with Fault Localization," *IEEE Transactions on Transportation Electrification*, vol. 11, no. 1, pp. 75–85, 2025, doi: 10.1109/TTE.2024.3386847.

[4] S. Han *et al.*, "In-Service Monitoring of Stator-Slot Magnetic Wedge Condition for Induction Motors," *IEEE Transactions on Industry Applications*, vol. 52, no. 4, pp. 2900–2910, 2016, doi: 10.1109/TIA.2016.2539128.

[5] M. Malekpour, B. T. Phung, and E. Ambikairajah, "Online technique for insulation assessment of induction motor stator windings under different load conditions," *IEEE Transactions on Dielectrics and Electrical Insulation*, vol. 24, no. 1, pp. 349–358, 2017, doi: 10.1109/TDEI.2016.006139.

[6] G. Mirzaeva, K. I. Saad, and M. G. Jahromi, "Comprehensive Diagnostics of Induction Motor Faults Based on Measurement of Space and Time Dependencies of Air Gap Flux," *IEEE Transactions on Industry Applications*, vol. 53, no. 3, pp. 2657–2666, 2017, doi: 10.1109/TIA.2016.2628718.

[7] Y. Yu, Y. Zhao, B. Wang, X. Huang, and D. Xu, "Current sensor fault diagnosis and tolerant control for VSI-based induction motor drives," *IEEE Transactions on Power Electronics*, vol. 33, no. 5, pp. 4238–4248, 2018, doi: 10.1109/TPEL.2017.2713482.

[8] X. Liang, "Temperature estimation and vibration monitoring for induction motors and the potential application in electrical submersible motors," *Canadian Journal of Electrical and Computer Engineering*, vol. 42, no. 3, pp. 148–162, 2019, doi: 10.1109/CJECE.2018.2875111.

[9] P. Y. Chen, K. H. Chao, and Y. C. Tseng, "A Motor Fault Diagnosis System Based on Cerebellar Model Articulation Controller," *IEEE Access*, vol. 7, pp. 120326–120336, 2019, doi: 10.1109/ACCESS.2019.2937103.

[10] M. Zafarani, B. H. Jafari, and B. Akin, "Lateral and Torsional Vibration Monitoring of Multistack Rotor Induction Motors," *IEEE Transactions on Industrial Electronics*, vol. 68, no. 4, pp. 3494–3505, 2021, doi: 10.1109/TIE.2020.2977547.

[11] B. D. E. Cherif, M. Chouai, S. Seninete, and A. Bendiabdellah, "Machine-Learning-Based Diagnosis of an Inverter-Fed Induction Motor," *IEEE Latin America Transactions*, vol. 20, no. 6, pp. 901–911, 2022, doi: 10.1109/TLA.2022.9757372.

[12] Q. Zhu *et al.*, "Real-Time Defect Detection of Die Cast Rotor in Induction Motor Based on Circular Flux Sensing Coils," *IEEE Transactions on Industrial Informatics*, vol. 18, no. 12, pp. 9271–9282, 2022, doi: 10.1109/TII.2021.3136560.

[13] Q. Zhu *et al.*, "Real-Time Quality Inspection of Motor Rotor Using Cost-Effective Intelligent Edge System," *IEEE Internet of Things Journal*, vol. 10, no. 8, pp. 7393–7404, 2023, doi: 10.1109/JIOT.2022.3228869.

[14] D. Garcia-Perez, M. Saeed, I. Diaz, J. M. Enguita, J. M. Guerrero, and F. Briz, "Machine Learning for Inverter-Fed Motors Monitoring and Fault Detection: An Overview," *IEEE Access*, vol. 12, pp. 27167–27179, 2024, doi: 10.1109/ACCESS.2024.3366810.

[15] A. C. S. Araújo, L. M. Rabelo, P. C. M. L. Filho, and W. M. Caminhas, "A Digital Twin Approach to Smart Monitoring and Fault Diagnosis," *IEEE Access*, vol. 13, pp. 148384–148395, 2025, doi: 10.1109/ACCESS.2025.3601349.

[16] R. A. K. Aswad, L. Szamel, and B. M. H. Jassim, "A Comprehensive Review of Fault Diagnosis and Prognosis Strategies for Three-Phase Induction Motors: 2010–2025," *IEEE Access*, vol. 13, pp. 201889–201903, 2025, doi: 10.1109/ACCESS.2025.3637859.

[17] Y. Miao, C. Yin, and B. Du, "Fault Diagnosis of Induction Motor Stator Windings Using an Improved PSO Algorithm," in *2025 5th International Conference on Intelligent Power and Systems (ICIPS)*, Xi'an, China, 2025, pp. 684-688, doi: 10.1109/ICIPS67876.2025.11332003.

[18] J. A. Toledo, L. A. R. Silva, and T. A. C. Maia, "Modeling of Three-Phase Induction Machines Under Combined Inter-Turn Fault and Mechanical Eccentricity," *IEEE Access*, vol. 13, pp. 178478–178491, 2025, doi: 10.1109/ACCESS.2025.3621153.

[19] H. Li, M. Gao, D. Xiang, C. Hu and B. Wang, "NonContact Monitoring of Stator Winding Temperature in Inverter-Fed Machines Using High-Frequency Switching Oscillations," *IEEE Transactions on Transportation Electrification*, vol. 12, no. 2, pp. 2514-2524, April 2026, doi: 10.1109/TTE.2026.3652237.

[20] P. M. Balasubramaniam, J. Sivakumar, S. Prabhu, A. V, V. Muniyan, and V. Madhaiyan, "Advancing Switched Reluctance Motor Design for Electric Vehicles Through Performance Optimization," in *2025 International Conference on Multi-Agent Systems for Collaborative Intelligence (ICMSCI)*, Erode, India, 2025, pp. 624-630, doi: 10.1109/ICMSCI62561.2025.10894310.

[21] K. Sreeram, C. M. Jacob, S. Cyril, A. R. Punnen, and J. James, "Optimization of Switched Reluctance Motor (SRM) Drive for Torque Ripple Mitigation and Cost Reduction in Plug-in Hybrid Electric Vehicle (PHEV)," in *2025 IEEE International Transportation Electrification Conference (ITEC-India)*, Pune, India: IEEE, 2025, pp. 1–6, doi: 10.1109/ITEC-India67626.2025.11439752.

[22] R. G. Shriwastava, M. P. Thakre, K. V. Bhadane, M. S. Harne, and N. B. Wagh, "Performance enhancement of DCMLI fed DTC-PMSM drive in electric vehicle," *Bulletin of Electrical Engineering and Informatics*, vol. 11, no. 4, pp. 1867–1881, 2022, doi: 10.11591/eei.v11i4.3714.

[23] B. Kumar, B. P. Panigrahi, and A. K. Panda, "Simulation studies on 2/3/5-level DTC based speed control of im drive in four quadrant Operation," in *2025 International Conference on Power Electronics Converters for Transportation and Energy Applications (PECTEA)*, IEEE, Ed., Jatni, India, 2025, pp. 1–6, doi: 10.1109/PECTEA61788.2025.11076230.
[24] S. Wang, Z. S. Zhang, Y. Hou, P. Liu, and Z. Wang, "Research on Plug-in Hybrid Electric Vehicle Bus Utility Factor Based on Real-World Data," in *2021 6th International Conference on Transportation Information and Safety (ICTIS)*, Wuhan, China: IEEE, 2021, pp. 799–804, doi: 10.1109/ICTIS54573.2021.9798549.
[25] P. Mishra, S. Rath, C. Badachi, S. Keshri, and U. Debnath, "Condition Monitoring of a 3-Phase Induction Motor," *8th International Conference on I-SMAC (IoT in Social, Mobile, Analytics and Cloud), I-SMAC 2024 - Proceedings*, pp. 359–365, 2024, doi: 10.1109/I-SMAC61858.2024.10714753.
[26] C. Ma, Z. Jiang, Z. Jia, and W. Song, "A Data-Driven Monitoring Method for Stator Insulation Degradation in Induction Motors Based on ConvNeXt Network," *IEEE Transactions on Energy Conversion*, vol. 40, no. 4, pp. 3163–3174, 2025, doi: 10.1109/TEC.2025.3565525.
[27] M. Z. Ali, M. N. S. K. Shabbir, S. M. K. Zaman, and X. Liang, "Single- And Multi-Fault Diagnosis Using Machine Learning for Variable Frequency Drive-Fed Induction Motors," *IEEE Transactions on Industry Applications*, vol. 56, no. 3, pp. 2324–2337, 2020, doi: 10.1109/TIA.2020.2974151.
[28] Y. Xia, Y. Xu, B. Gou, and Q. Deng, "A Learning-Based Method for Speed Sensor Fault Diagnosis of Induction Motor Drive Systems," *IEEE Transactions on Instrumentation and Measurement*, vol. 71, pp. 1–10, 2022, doi: 10.1109/TIM.2021.3132053.
[29] P. Narasimman, A. S. Tharsha, M. Abirami, S. Uma, and U. Harini, "IoT Based IGBT Power Module Health Monitoring with RUL Estimation in Electric Vehicle Applications," in *2026 International Conference on Innovations in Emerging Technologies for Sustainable Development (ICIETSD)*, Pudukkottai, India, 2026, pp. 1-7, doi: 10.1109/ICIETSD68684.2026.11584677.
[30] M. E. A. Khodja, A. H. Boudinar, and A. F. Aimer, "Improvement of Induction Motor Diagnosis using the Kaiser Window Function," in *2023 International Aegean Conference on Electrical Machines and Power Electronics (ACEMP) & 2023 International Conference on Optimization of Electrical and Electronic Equipment (OPTIM)*, Istanbul, Turkiye: IEEE, 2023, doi: 10.1109/ACEMP-OPTIM57845.2023.10287081.

BIOGRAPHIES OF AUTHORS

Dr. Mohan P. Thakre received the B.Tech. and M.Tech. degrees in Electrical Power Engineering from Dr. Babasaheb Ambedkar Technological University (Dr. BATU), Maharashtra, India, in 2009 and 2011 respectively, and the Ph.D. degree in Electrical Engineering from Visvesvaraya National Institute of Technology (VNIT), Nagpur, Maharashtra, India in 2017. Currently, he is an associate professor at the Department of Electrical Engineering, Walchand College of Engineering, Sangli, Maharashtra, India. His research interests include FACTS and power system protection and renewable energy. He can be contacted at email: mohanthakre@gmail.com.

Dr. Badal Kumar received his B.Tech. in Electrical and Electronics Engineering from Biju Patnaik University of Technology (2011) and M.E. in Digital Techniques and Instrumentation from S. G. S. Institute of Technology and Science (2015). He completed his Ph.D. from National Institute of Technology Manipur in 2022. He began his academic career in 2015 and served at Oriental College of Technology and Medi-Caps University. After his Ph.D., he worked at K. K. Wagh Institute of Engineering Education and Research, Shreeyash College of Engineering and Technology, and SVERI's College of Engineering in various academic and leadership roles. Currently, he is an Associate Professor in the Department of Electrical Engineering at JSPM University. His research interests include microgrids, smart grids, power system control, metaheuristic algorithms, AI, and renewable energy systems. He can be contacted at email: kumarbadal89@gmail.com.

Dr. Supriya Nilesh Thakur is currently serving as an Assistant Professor in the Department of Electrical Engineering at Marathwada Mitra Mandal's College of Engineering, Karvenagar, Pune, Maharashtra. She is actively involved in teaching, academic development, and research activities in the field of Electrical and Electronics Engineering. She has completed her Bachelor's degree in Electronics Engineering from Rajarambapu Institute of Technology, Sakharale, Islampur, Maharashtra, India. She pursued her Master's degree in Electronics and Telecommunication Engineering from MGM College of Engineering, Kalamboli, Panvel, Navi Mumbai, Maharashtra. Further strengthening her academic and research credentials, she completed her Ph.D. in Electrical and Electronics Engineering from the Sandip University, Nashik, Maharashtra, under the School of Engineering and Technology (SOET). She has a strong passion for teaching and mentoring students in core electrical and electronics subjects. Her research interests mainly focus on photovoltaic modules and their electrical parameters. She can be contacted at email: supriyathakur@mmcoe.edu.in.

Dr. Alok Kumar received his B.Tech. degree in Electrical and Electronics Engineering from Biju Patnaik University of Technology, Rourkela, Odisha, in 2012. He completed his M.Tech. from the National Institute of Technology (NIT), Hamirpur, India, in 2015, and earned his Ph.D. from the Indian Institute of Technology (Indian School of Mines), Dhanbad, India. He has more than seven years of teaching experience in various engineering colleges across India. Currently, he is working as an Associate Professor in the Department of Electrical Engineering at SVERI's College of Engineering, Pandharpur, District Solapur, India. He current research interests include condition monitoring of electrical power apparatus and power system analysis. He can be contacted at email: kumaralok340@gmail.com.

Dr. Padmini Sharma is an Associate Professor and Head of the Department of Electrical and Electronics Engineering at Chhatrapati Shivaji Institute of Technology, Durg, with over 21 years of teaching experience. She completed her B.E. in Electrical Engineering (2003) and M.Tech. in Instrumentation and Control (2008) from Bhilai Institute of Technology. She earned her Ph.D. in 2019 from C.V. Raman University for her research on numerical protective relays in power system oscillations. She also completed an M.Sc. in Mathematics (2024) and a Postgraduate Certificate in Data Science from IIT Bhilai (2025). She is a Life Member of ISTE, has completed several NPTEL courses, and received the "Discipline Star" award. Her research focuses on power system protection and stability analysis. She can be contacted at email: padminisharma@csitdurg.in.

Dr. Prashant Kedarnath Magadum received his B.E. Electrical Electronics and Power Engineering from Swami Ramanand Teerth Marathawada University, Nanded, Maharashtra, India and M.E. Electrical (Power System) from Shivaji University, Kolhapur, Maharashtra, India respectively. He had completed Ph.D. degree in Electrical and Electronic Engineering from Visvesvaraya Technological University, Belgum, Karnataka, India. He is currently working as Associate Professor and Head, Department of Electrical Engineering, Brahmadevdada Mane Institute of Technology, Solapur, Maharashtra, India. He has having more than 20 years of teaching experience and has published more than 4 papers in various national and international journals. His research interest includes the design and control of multilevel converters for grid applications, FACTS based on modular multilevel converters and its controls. He can be contacted at email: magadumpk@gmail.com.